voids produced in the crystal during fabrication can change shape and volume as atoms migrate under various circumstances. As shown above, the smallest voids tend to remain rounded in shape due to the dominant influence of surface energy over elastic energy. However, larger voids can become elongated and eventually develop into fractures. This is more likely to occur under uniaxial stress than under the conditions of equi-biaxial stress that were assumed for purposes of illustration here.

8.4 Periodic perturbation of a flat surface

Suppose that, in its reference configuration, an elastic material has a nominally flat surface that is free of applied traction. If the solid is then stressed, is the flat surface shape stable under perturbations in shape? These perturbations are changes in the reference configuration of the material that are achieved by rearrangement of mass, and are not a consequence of deformation of the material. The question is addressed in this section for the case of periodic perturbation of surface shape. Perturbations of very small amplitude are considered first, and this discussion is followed by consideration of higher order effects and substrate stiffness. Cases of nonperiodic surface perturbations are considered in the following section.

8.4.1 Small amplitude sinusoidal fluctuation

An isotropic elastic solid with a nominally flat, traction-free surface is subjected to an initial equilibrium stress field. Suppose that the shape of the free surface S' in the undeformed reference configuration of the material is not actually a plane but that it is slightly wavy. The nominally flat surface coincides with the plane $y = 0$ and the position of the actual surface varies with respect to $y = 0$ in the x-direction. At time t, the position of the surface at coordinate x is given by $y = h(x, t)$. For the discussion in this section, it is assumed that the slope of the surface is small everywhere, that is, $|h_{,x}| \ll 1$ at all points on the surface. The boundary condition that must be enforced on the wavy surface is that the traction is zero.

If σ_{ij} is the stress field evaluated at a point on the surface and n_j is the outward unit normal vector there then $\sigma_{ij}n_j = 0$ at that point. This condition must be enforced pointwise on the wavy surface, and this will be done for the case of small amplitude surface slope. A sketch of a small portion of the surface is shown in Figure 8.10. To lowest order in surface slope, the vector n_i has components $n_x \approx -h_{,x}$, $n_y \approx 1$. The tangential direction on the surface is then given by the unit vector s_i which has components $s_x = n_y$ and $s_y = -n_x$. The normal traction on the surface with unit normal vector n_i corresponding to boundary values of stress defined by its tensor components σ_{ij} in rectangular coordinates is $\sigma_n = n_i\sigma_{ij}n_j$. Similarly, the shear

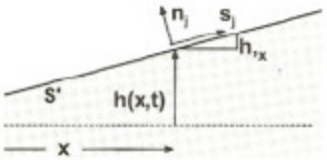

Fig. 8.10. The shape of a material surface in its reference configuration is described by means of its normal distance $h(x, t)$ from a reference plane at place x and time t. The unit vectors s_j and n_j specify directions locally tangent and normal to the surface.

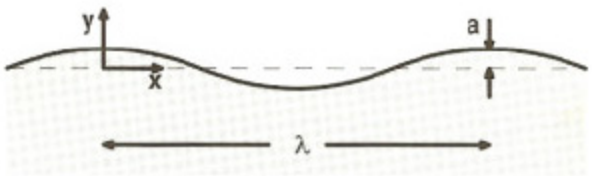

Fig. 8.11. Schematic diagram of the nominally flat material surface which deviates sinusoidally from the mean surface position. Surface deviation is described by (8.47), and the amplitude-to-wavelength ratio a/λ is assumed to be small.

traction is $\sigma_s = s_i \sigma_{ij} n_j$. Both σ_n and σ_s must vanish on $y = h(x, t)$ if the surface is to be free of applied traction. When expanded to first order in the magnitude of the surface slope, these conditions become

$$\begin{aligned} &\sigma_{yy}(x, h) - 2h_{,x}\, \sigma_{xy}(x, h) = 0\,, \\ &h_{,x}\, \sigma_{xx}(x, h) - h_{,x}\, \sigma_{yy}(x, h) - \sigma_{xy}(x, h) = 0\,. \end{aligned} \tag{8.44}$$

Prior to perturbation of surface shape, an equilibrium state of stress $\sigma_{ij}^{(0)}(x, y)$ exists in the material with the surface $y = 0$ being traction-free. The total stress field for the perturbed shape of the surface is of the form

$$\sigma_{ij}(x, y) = \sigma_{ij}^{(0)}(x, y) + \sigma_{ij}^{(h)}(x, y)\,. \tag{8.45}$$

Then (8.44) indicates that the boundary conditions on the *additional* stress field $\sigma_{ij}^{(h)}(x, y)$ due to perturbation of the shape of the free surface to $y = h(x, t)$ will be

$$\sigma_{yy}^{(h)}(x, h) - 2h_{,x}\, \sigma_{xy}^{(0)}(x, 0) = 0\,, \quad h_{,x}\, \sigma_{xx}^{(0)}(x, 0) - \sigma_{xy}^{(h)}(x, h) = 0\,. \tag{8.46}$$

Nonetheless, the analysis is pursued on the basis of the boundary conditions in the form (8.44).

To make the discussion more concrete, suppose that the surface shape is sinusoidal in the x-direction with wavelength $\lambda > 0$ and amplitude $a > 0$, so that

$$h(x, t) = a \cos \frac{2\pi x}{\lambda} \tag{8.47}$$

as indicated in Figure 8.11. The shape is uniform in the z-direction. The restriction

to surface shapes with small slope implies that $a/\lambda \ll 1$. The goal is to find the perturbation of the initial equilibrium stress field $\sigma_{ij}^{(0)}(x, y)$, denoted by $\sigma_{ij}^{(h)}(x, y)$ above, that is required to enforce the boundary conditions (8.44). For the time being, suppose that the initial stress state is spatially uniform and that it results from a remotely applied equi-biaxial tensile stress of magnitude σ_m acting in the direction parallel to the surface. In this case,

$$\sigma_{xx}^{(0)}(x, y) = \sigma_m \quad \text{and} \quad \sigma_{xy}^{(0)}(x, y) = \sigma_{yy}^{(0)}(x, y) = 0 \tag{8.48}$$

throughout the material.

For a sinusoidal perturbation of shape as given by (8.47) and for a uniform initial stress field, the additional elastic stress is also expected to be sinusoidal in x for fixed y. The stress field has the appropriate symmetry if it is derived from an Airy stress function of the form

$$A(x, y) = f(y) \cos \frac{2\pi x}{\lambda}, \tag{8.49}$$

where $f(y)$ is a function of y which is to be determined. The stress function A must satisfy the biharmonic equation, which ensures both that the stress field is an equilibrium field and that the associated strain field is compatible (Timoshenko and Goodier 1987). Furthermore, all stress components must vanish as $y \to -\infty$, which implies that

$$f(y) = \left(c_0 + c_1 \frac{y}{\lambda}\right) e^{2\pi y/\lambda} \tag{8.50}$$

where c_0 and c_1 are constants to be determined by enforcing of the boundary conditions. If the components of stress $\sigma_{ij}^{(h)}(x, y)$ are derived from (8.49) according to (6.3), and if the boundary conditions (8.44) are enforced for $y = h = a \cos(2\pi x/\lambda)$, then it is found that

$$c_0 = 0, \quad c_1 = -a\lambda\sigma_m \tag{8.51}$$

to first order in a/λ. The corresponding stress components along the surface are

$$\sigma_{xx}^{(h)} = -\frac{4\pi a}{\lambda}\sigma_m \cos \frac{2\pi x}{\lambda}, \quad \sigma_{yy}^{(h)} = 0, \quad \sigma_{xy}^{(h)} = 0. \tag{8.52}$$

It can be seen immediately from (8.52) that, as a increases from zero, the stress at the peaks ($x = 0, \pm\lambda, \ldots$) decreases in magnitude from the initial value σ_m and that the stress at the valleys in the surface profile ($x = \pm\lambda/2, \pm 3\lambda/2, \ldots$) increases in magnitude from the initial value σ_m.

The strain energy density along the surface, accurate to first order in the small parameter a/λ, is then

$$U(x) = U_{\mathrm{m}}\left[1 - 4\pi(1+\nu)\frac{a}{\lambda}\cos\frac{2\pi x}{\lambda}\right], \tag{8.53}$$

where

$$U_{\mathrm{m}} = \frac{\sigma_{\mathrm{m}}^2}{M} \tag{8.54}$$

is the uniform strain energy density of the remote field; $M = E/(1-\nu)$ is the biaxial elastic modulus expressed in terms of the elastic modulus E and Poisson ratio ν.

The local increase in area of the surface due to the perturbation in shape is approximately

$$\tfrac{1}{2}h_{,x}(x,t)^2 = 2\pi^2\frac{a^2}{\lambda^2}\sin^2\frac{2\pi x}{\lambda}, \tag{8.55}$$

which is of second order in a/λ, and the local curvature is approximately

$$\kappa = h_{,xx}(x,t) = -4\pi^2\frac{a}{\lambda^2}\cos\frac{2\pi x}{\lambda}. \tag{8.56}$$

The chemical potential (8.8) then varies along the surface according to

$$\chi = U_{\mathrm{m}} + 4\pi\frac{a}{\lambda}\left[\frac{\pi}{\lambda}U_{\mathrm{S}} - (1+\nu)U_{\mathrm{m}}\right]\cos\frac{2\pi x}{\lambda}. \tag{8.57}$$

Thus, the surface chemical potential varies in phase (out of phase) with the perturbation in shape when $\pi U_{\mathrm{S}}/\lambda - (1+\nu)U_{\mathrm{m}} > 0$ (< 0). This is the condition that discriminates between stable and unstable surface perturbations. To see this, let a be time-dependent and note that

$$v_n = \dot{a}\cos\frac{2\pi x}{\lambda} \tag{8.58}$$

for small a/λ. Then the rate of change of free energy per period is approximately

$$\dot{\mathcal{F}}(t) = \int_0^{\lambda}\chi v_n\,dx = 2\pi a\dot{a}\left[\frac{\pi}{\lambda}U_{\mathrm{S}} - (1+\nu)U_{\mathrm{m}}\right], \tag{8.59}$$

where the natural length parameter

$$\zeta = \frac{U_{\mathrm{S}}}{U_{\mathrm{m}}} \tag{8.60}$$

again emerges. Therefore, for any small amount of waviness represented by $a > 0$, the system can lower its free energy by moving toward a configuration with a flat surface ($\dot{a} < 0$) if $\pi U_{\mathrm{S}}/\lambda > (1+\nu)U_{\mathrm{m}}$. On the other hand, if $\pi U_{\mathrm{S}}/\lambda < (1+\nu)U_{\mathrm{m}}$,

it can lower its free energy by increasing the amplitude of its waviness ($\dot{a} > 0$). A nominally flat surface is said to be stable under perturbations in surface shape in the former case and to be unstable in the latter case.

For a given set of system parameters U_S, E, ν and σ_m, the discriminating wavelength or *critical wavelength* is

$$\lambda_{cr} = \frac{\pi U_S}{(1+\nu)U_m} = \frac{\pi U_S \bar{E}}{\sigma_m^2} \,. \tag{8.61}$$

A surface with sinusoidal perturbation of its nearly flat surface with wavelength that is less (greater) than λ_{cr} is stable (unstable) against spontaneous growth of the perturbation amplitude. For a surface energy density of $U_S = 1\,\mathrm{J\,m^{-2}}$, a plane strain modulus of $\bar{E} = 10^{11}\,\mathrm{N\,m^{-2}}$ and an applied stress of $\sigma_m = 10^9\,\mathrm{N\,m^{-2}}$, this critical wavelength λ_{cr} is approximately 300 nm.

Note that the critical wavelength in (8.61) depends on stress σ_m only through σ_m^2. As a result, the system behavior depends on the magnitude of stress but not on its algebraic sign, that is, the behavior under tension and compression are indistinguishable according to (8.61). This is at variance with observed behavior, where materials with $\sigma_m < 0$ behave in the way described here but systems with $\sigma_m < 0$ do not consistently do so (Xie et al. 1994). This question is re-examined in Section 8.8.3 on the basis of a surface energy density that depends on surface orientation in a way dictated by the fundamental nature of crystals.

The stability of a nominally flat bounding surface of a stressed solid was investigated independently by Asaro and Tiller (1972), Grinfeld (1986) and Srolovitz (1989). The instability was first observed and described qualitatively in solid ^{4}He by Bodensohn et al. (1986). Subsequently, Torii and Balibar (1992) developed an experiment that made it possible to induce the instability in solid ^{4}He under controlled conditions and to interpret the observations quantitatively. They determined equilibrium shapes, showing surface waviness, of the interface between a pure helium crystal and a helium vapor at very low temperature. This was done by imposing a variable applied stress on the crystal by means of piezoelectric end walls of its centimeter scale container. The surface shape was monitored by directing light onto the crystal and correlating patterns obtained due to interference of light reflected from both the top surface of the crystal and the mirrored bottom surface of its container with surface shape. In the growth of epitaxial semiconductor films that have a lattice mismatch with respect to their substrates, stresses sufficiently large to induce surface instability are readily achieved through the constraint of epitaxy. A particular case is described in the next example.

8.4.2 Example: Stability of a strained epitaxial film

A $Si_{0.81}Ge_{0.19}$ alloy film is grown epitaxially on a (001) surface of the Si substrate. Estimate the critical wavelength λ_{cr} as defined in (8.61) for the nominally flat growth surface of the film. Base the calculation on the values of elastic constants given in Table 3.1 and the surface energy value of $U_S = 1.2\,\mathrm{J\,m^{-2}}$ for the alloy.

Solution:

The mismatch strain between the film and substrate is approximated as described in (1.15) for a Ge concentration of $x = 0.19$, with the result that

$$\epsilon_m = -0.04 \times 0.19 = -0.0076\,. \tag{8.62}$$

The elastic constants to use with the isotropic model are estimated in terms of the constants for single crystal Si and Ge given in Table 3.1 by assuming that the waviness is aligned with a ⟨100⟩ direction. In this case, the elastic modulus and Poisson ratio values of both Si and Ge are determined according to

$$E = 1/s_{11} \quad \text{and} \quad \nu = -s_{12}/s_{11}\,. \tag{8.63}$$

Then, applying the linear rule of mixtures for the alloy, it follows that $E_{SiGe} = 125$ GPa and $\nu_{SiGe} = 0.276$. The mismatch stress is then

$$\sigma_m = \frac{E_{SiGe}}{1 - \nu_{SiGe}}\epsilon_m = -1.31\ \mathrm{GPa}\,. \tag{8.64}$$

The value of critical wavelength is estimated from (8.61) to be

$$\lambda_{cr} = \frac{\pi \times 1.2 \times 1.25 \times 10^9}{(1 - 0.276^2) \times 1.31^2 \times 10^{18}} = 296\,\mathrm{nm}\,. \tag{8.65}$$

A cross-sectional transmission electron microscopy image of a $Si_{0.81}Ge_{0.19}$ alloy film that was grown on the (001) surface of the Si substrate is shown in Figure 8.12. The growth temperature was 750 °C and mean film thickness is approximately 50 nm. The ripples on the surface are aligned with a ⟨100⟩ direction of the material. The wavelength of the more or less periodic surface profile is approximately 315 nm. Evidently, the amplitude-to-wavelength ratio of the surface profile is not small compared to unity, but the wavelength agrees reasonably well with the value estimated in this example. The surface profile is also not a simple sinusoid but, instead, it is sharpened in the valleys, flattened at the peaks and nearly linear between the valleys and peaks. The influence of higher order effects on perturbed shape will be considered in Section 8.4.4, and aspects of the profile arising from other effects will be discussed later in this chapter and in the next chapter.

8.4.3 Influence of substrate stiffness on surface stability

In the foregoing discussion of stability of the flat surface of a stressed solid, it was assumed that the elastic material is homogeneous. It was also assumed that, prior to formation of fluctuations in surface shape, the material was homogeneously stressed, that is, the equi-biaxial stress σ_m acted throughout the material. This assumption on

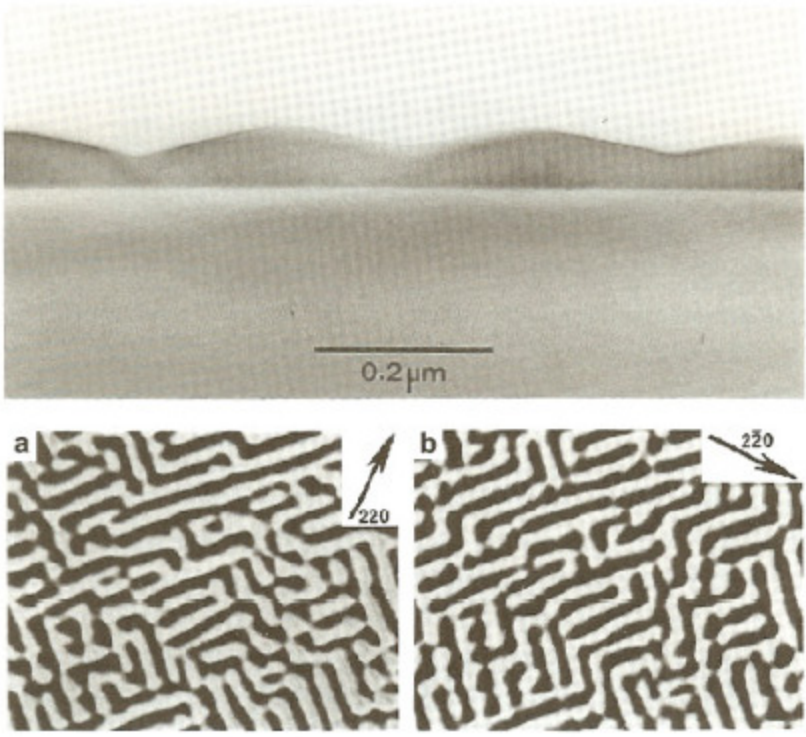

Fig. 8.12. Transmission electron microscopy cross-sectional image of a $Si_{0.81}Ge_{0.19}$ alloy film grown epitaxially on a Si substrate (top). The ridges are aligned with a ⟨100⟩ crystallographic direction. While the upper image appears to represent a fully two-dimensional configuration, the plan-view images of the film surface in the lower portion of the figure show that the regular ordering has a relatively short range. The normal distance between parallel lines in the lower images is the peak-to-peak distance in the upper image, or about 300 nm. Reproduced with permission from Cullis et al. (1992).

stress is not essential. It will be shown in Section 8.9 that the results are unaffected if the initial mismatch stress acts only to some finite depth, provided only that this depth extends beyond the roots of the valleys in surface fluctuation. Otherwise, a discontinuity in the initial stress across some plane $y =$ constant is immaterial. Discontinuities in elastic properties, however, do have an influence on stability.

Suppose that a film of thickness h is epitaxially bonded to a substrate with relatively large thickness. Both materials are assumed to be homogeneous and isotropic elastic materials, but with different elastic moduli, so that $E_s \neq E_f$. For simplicity, the two materials are assumed to have the same Poisson ratio, that is, $\nu_f = \nu_s = \nu$. The film is subjected to a homogeneous equi-biaxial stress σ_m when the free surface is flat and the substrate is initially stress-free. The central question again concerns the stability of the flat surface under sinusoidal perturbations of its shape resulting from mass rearrangement.

Fig. 8.36. Island shape transitions are represented in Figure 8.35 under the assumption that only abrupt transitions from one conical shape with relatively small aspect ratio a_1 to another with relatively large aspect ratio a_2 are possible. This diagram suggests a more gradual transition from one conical shape to another, effected by having the steeper orientation a_2 gradually expand on the lateral face of the island until the transition is completed.

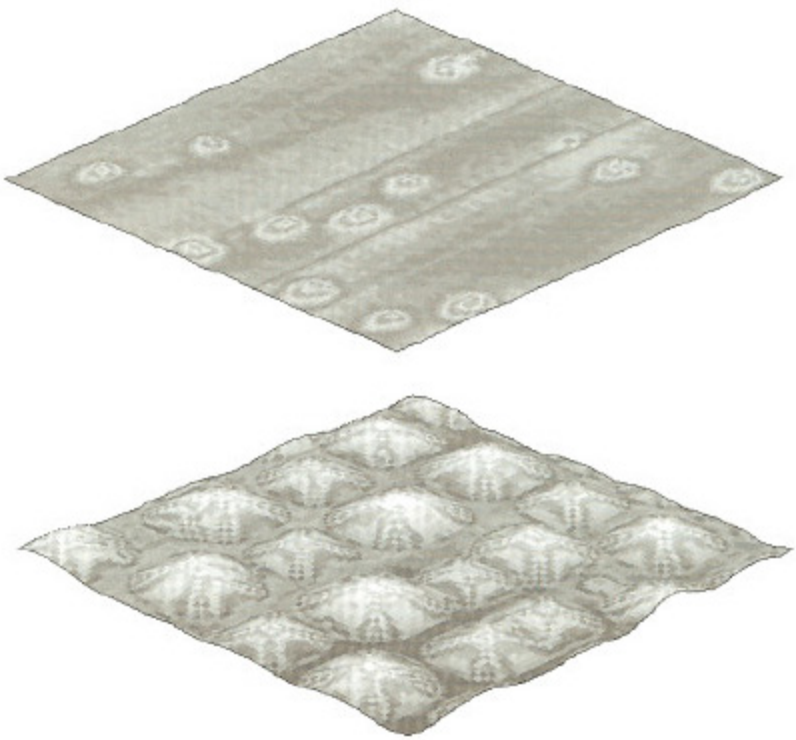

Fig. 8.37. Surface profiles of $Si_{0.8}Ge_{0.2}$ grown epitaxially on the (001) surface of a Si substrate at 755 °C obtained by means of atomic force microscopy. The plan view area of each image is 2 μm×2 μm, and the vertical scales are identical. The mean deposition depths are 25 Å in the upper image, where widely spaced incipient islands are evident, and 100 Å in the lower image, where an array of islands with {105} lateral faces has been formed. Reproduced with permission from Floro et al. (1997, 1998).

8.9.6 Observations of island formation

Images of islands that formed spontaneously during deposition of the alloy $Si_{0.8}Ge_{0.2}$ on Si(001) at 755 °C, obtained by means of atomic force microscopy after the deposition was interrupted, are shown in Figure 8.37. The upper image shows very small

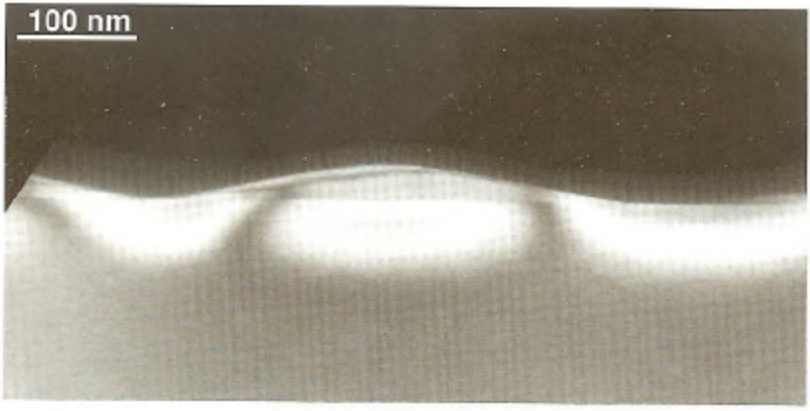

Fig. 8.38. Cross-sectional image of one of the islands in the lower portion of Figure 8.37, obtained by means of transmission electron microscopy. The lateral faces of the island are {105} surfaces, typical for this material system. Reproduced with permission from Floro et al. (1997).

islands forming on the growth surface during the early stage of deposition. In the lower image, islands have grown nearly to the point of mutual impingement. The edges of the square island bases are aligned with ⟨100⟩ directions on the growth surface. Note that the lateral faces of the islands all have approximately the same slope. An enlarged view of a cross-section of one of the islands in the lower portion of Figure 8.37, obtained by transmission electron microscopy, is shown in Figure 8.38. This image reveals that the lateral faces of the island appear to be {105} surfaces.

The evolution of island shapes and the transition from a pyramidal shape to a dome shape has been studied in detail for the SiGe/Si(001) material system by Ross et al. (1999). The observations were carried out in an apparatus that integrated low energy electron microscopy (LEEM) with *in situ* film growth capabilities. Geometrical features of evolving island configurations are distinguishable in LEEM images due to their relatively strong contrast. The shape transition for $Si_{0.75}Ge_{0.25}$ deposited at 730 °C is summarized in Figure 8.39. The flat growth surface in this case is unstable as described in Section 8.9.3, and the deposit agglomerates into islands with vicinal lateral faces approaching the {105} orientation, the so-called pyramidal (P) shape. As the island becomes larger in volume, it transforms to a truncated pyramid (TP) shape as {113} faces appear at the corners of the square base and grow in area; a schematic of the TP shape is illustrated on the right in Figure 8.39. Once the {113} faces become fully established, additional faces emerge which appear to flatten edges at face boundaries to a certain extent. The configuration proceeds through successive dome-like shapes (D1, D2, D3) until the final shape D4 is reached, consisting of {113} and {15 3 23} lateral surfaces plus remnants of the {105} faces at the top. The transitions all appear to be temperature dependent.